ADVANCED MATERIALS TECHNOLOGIES
www.advmattechnol.de

Additive Manufacturing of Columnar Thermal Barrier Coatings by Laser Cladding of Ceramic Feedstock

*Christoph Vorkötter, Daniel Emil Mack, Robert Vaßen, and Olivier Guillon**

This study presents a new laser-cladding-based additive manufacturing technique named Clad2Z. Using a robot-mounted confocal powder nozzle with axial infrared laser beam, ceramic columns with a diameter of 450 µm and an adjustable height are developed. Influence of laser parameters and robot movements on shape and microstructure is analyzed. As an example application, the common material yttria-stabilized zirconia (YSZ) is used to deposit columnar-structured thermal barrier coatings (TBCs). The excellent thermal cycling performance of the Clad2Z samples is demonstrated by burner rig tests and comparing lifetime and failure mechanism with conventional TBC systems.

1. Introduction

Laser cladding manufacturing technology combines a laser heat source with computer-controlled robotics and powder metallurgy. It is conventionally used to deposit metal layers. Bulk metal components can be manufactured by using slicing technology, as the component is built in several individual layers. The layer material is transferred to the substrate either by powder injection, pre-placed powder or wire feeding, while powder injection is described as the most effective method.[1] A characteristic of the process is that the substrate is somewhat molten and the powder is added to this molten pool.

C. Vorkötter, D. E. Mack, R. Vaßen, O. Guillon
Institute of Energy and Climate Research – Materials Synthesis and Processing (IEK-1)
Forschungszentrum Jülich GmbH
Wilhelm Johnen Straße, 52425 Jülich, Germany
E-mail: o.guillon@fz-juelich.de

R. Vaßen
Institute for Materials
Ruhr-Universität Bochum
44780 Bochum, Germany

O. Guillon
Jülich Aachen Research Alliance
JARA-ENERGY
52425 Jülich, Germany

The ORCID identification number(s) for the author(s) of this article can be found under https://doi.org/10.1002/admt.202200098.

DOI: 10.1002/admt.202200098

Among the laser cladding coating applications, metal, or metal alloy powders are mostly used for wear-resistance coatings, repair coatings, or coatings with increased hardness.[2] One of the common laser cladding systems with powder injection uses coaxial powder feeding and has the advantage of cladding independent of the moving direction. Laser cladding with metal powder on a metal substrate has been used for several decades for turbine blade repairs in particular, for example, at its tip.[1] Changing the material to ceramics, especially when cladding ceramics on metal, the formation of cracks during processing is almost inevitable due to high residual stress from the solidification shrinkage, caused by local and temporal temperature gradients, and the thermal expansion coefficient mismatch between the coating and the substrate.[3,4] These cracks are one main reason for minor interest in ceramic laser cladding compared to metallic laser cladding. Some ceramic layers and their applications are presented in the literature for wear-resistant coatings[5] or even for thermal barrier coatings (TBCs) by linear scanning in the horizontal plane of the substrate. However, these coatings are characterized by significant cracking and inhomogeneities.

TBCs for super alloy structural parts such as turbine blades and vanes typically consist of a porous ceramic top coat on a dense metallic bond coat. The main purpose of the porous top coat is to insulate heat. If the substrate is cooled from the backside, the low thermal conductivity of the top coat maintains a thermal gradient from the surface of the protective coating to the protected material. The bond coat protects the substrate from oxidation and enhances the adhesion of the top coat. A key factor influencing the thermal cycling performance of the TBC system is the thermal expansion coefficient mismatch between the top coat and the bond coat leading to stresses during thermal cycling. To tackle this issue, columnar-structured coatings offer enhanced strain tolerance and thus enhanced thermal cycling performance.[6,7] Common techniques for manufacturing columnar TBCs are plasma spray physical vapor deposition (PS-PVD) or suspension plasma spaying (SPS). For these manufacturing techniques, column growth is caused by different growth rates from the vapor phase and by shielding the particle flow at surface undulations, respectively.

Laser cladding for TBCs is used due to its similar diameter of 100–400 µm of features in columnar suspension plasma sprayed TBCs, and the size of the laser clad structures known from the literature. When separate columns are produced by laser cladding, the formation of cracks due to thermomechanical stresses

can in principle be suppressed – even for completely dense columns, if they have a sufficiently small cross section. At the same time, when these columns are densely packed, a thermal barrier layer with a high strain tolerance and a flexible height can be produced. In this study, the moving direction of the laser cladding system was extended from the conventional horizontal (x–y direction) direction along the substrate plane to the lateral moving direction (z-direction), named "Clad2Z". Moving the laser cladding system in a lateral direction relative to the substrate surface plane, dense, crack-free columnar ceramic structures, and promising 3D structures were manufactured. Some variation in the processing parameters enabled the production of homogeneous columns and – column by column – coatings with high lateral resolution. Columns were first grown on atmospheric plasma sprayed YSZ (APS YSZ) coatings on steel. For thermal cycling performance tests a conventional bond coat layer was added, and the substrate was changed to a common gas turbine blade material Inconel 738 (IN738).

2. Results and Discussion

2.1. Column Laser Cladding on YSZ Using Clad2Z

As described in the introduction, the aim of this work is to produce columnar TBCs based on the sequential generation of individual columns by means of laser cladding. For this purpose, the processing head of a coaxial laser cladding nozzle is moved away from the component surface in a way that results in the laser beam causing a narrowly confined melt pool. From this melt pool, a column can be built up by the powder feed. This implies that the melt pool is formed initially in the plane of the component surface, but the column is built up at the top of the column in the further course of the process (**Figure 1**). In particular, while generating the initial melt pool at the surface of the component, the heat-affected zone needs to be kept small by precisely adjusting the heat input. As the process progresses, the extent of the melt pool is closely related to the heat conduction and geometry of the YSZ column that builds up.

Initially, a thin layer of YSZ deposited using the APS method was chosen as a substrate. This choice was related its similarity to the structure of columnar TBCs produced using the SPS process. It was also motivated by the desire to develop a repair process for only partially or locally ablated TBCs.

In general, the processing of YSZ by Nd:YAG infrared laser radiation is difficult, since the YSZ ceramic absorption is low in the near-infrared (NIR) light spectrum and a high proportion of incident radiation is reflected due to a comparatively high refractive index (coefficient of absorption $a_{1\mu m} < 0.1$ cm^{-1}, coefficient of scattering $\sigma_{1\mu m} > 1000$ cm^{-1}).[8] While the scattering power shows no significant temperature dependence, there is a regular increase with temperature for the absorption, although at temperatures of 1360 °C, for example, the absorption $a_{1\mu m} < 10$ cm^{-1} is well below the scattering coefficient.[9] In plasma-sprayed TBC layers with a typically high number of (sub)micrometer-scale pores, diffuse scattering causes increased absorption and reflection and thus reduced transmission due to multiple reflections at the pore interfaces. For example, a typical TBC layer with a thickness of 300 µm and ≈10% porosity exhibits a reflectivity in the order of 85% at room temperature, while transmission is in the order of 10%, and absorption is <5%.[10] However, the specific values depend significantly on the microstructure, and reflectivities of up to 95% have been reported for very fine-porous TBCs.[11]

Despite the low absorptivity of YSZ in the NIR, we observed in a prior study on the cladding of metallic sensors, that only superficial melting of TBC was achieved for a moderate energy input of ≈10 J mm^{-1}.[12] This could be attributed to the fact that the diffuse broadening and backscattering of the laser beam in the porous coating effectively caused increased energy absorption in the near-surface volume. In the same study, it was also confirmed that the laser power at the substrate surface level could be noticeably reduced by scattering from coaxially fed particles.[13]

With this in mind, a laser focused to 20 µm was used in the current study, to achieve processing dimensions of the same or a smaller order of magnitude than that of the focus diameter of the coaxial powder feed of ≈200 µm, even with the expected widening of the beam. The focal plane of the laser and powder feed were aligned and initially positioned 1 mm below the substrate surface at the start of the welding process in order to prevent additional scattering on the feedstock

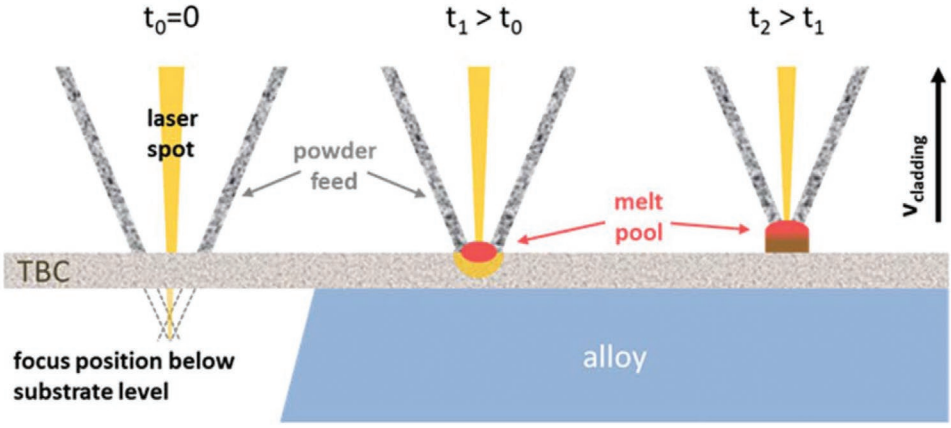

Figure 1. Principle of Clad2Z vertical laser cladding on porous zirconia (zirconia thickness 500 µm) powder focus (0.2 mm diameter, 3.6 g min^{-1}) and infrared laser focus (0.02 mm diameter, 20 W continuous wave) are aligned, $v_{cladding}$ = 5–60 mm s^{-1} in *z*-direction

particles at this point (Figure 1 $t_0 = 0$). The powder focal plane and laser focal plane will be simply referred to as "focal plane" from here on in the purpose of better legibility. The powder feedstock was fed into the central processing zone after a delay in the course of the vertical movement of the processing head – ideally after a surface melt pool had been formed (Figure 1 $t_1 > t_0$). In accordance with the study of Zhang et al., a low laser power of 20 W and a high powder feed rate of 3.6 g min^{-1} (20 l min^{-1} carrier gas) were used. The gas flow and powder feed were turned on prior to laser processing until a stable powder flow was visible. Gas flow and powder feeding were maintained throughout the processing time to keep the powder flow constant.

We infer that after the formation of a surfacial melt pool, the extension of the melt pool into the substrate or the buildup of a column is primarily controlled by the heat conduction in the substrate and the energy demand for melting the YSZ. The latter can be estimated as $H_{min} = c_p \times (T_{melt} - T_{RT}) + H_{fusion} = 2330$ J g^{-1} ($c_p = 0.61$ J g^{-1} K^{-1}, $T_{melt} = 2950$ K, $H_{fusion} = 710$ J g^{-1}). Accordingly, for the buildup of a column with a powder focus diameter of 200 µm, at least ≈0.3 J will have to be supplied by the laser to form the initial melt pool (from 10 J mm^{-1}) and an additional ≈0.4 J mm^{-1} as a function of the build height (YSZ ≈6 g cm^{-3}). With this energy demand, the minimum building energy of a 5 mm column (with 200 µm diameter) is ≈2.4 J. In fact, noticeably higher values are expected in real experiments due to losses from scattering, heat dissipation, or overheating of the melt and potential widening of the structure.

With this energy demand in mind, the first experiments were set so that the energy provided by the laser could be varied. This was achieved by varying the robot velocity set for a vertical movement (processing distance) of $\Delta_z = 6$ mm. The velocities (v_z) were set to 60, 20, 10, and 5 mm s^{-1}, corresponding to 2, 6, 12, and 24 J of energy provided using 20 W of laser power and assuming a constant robot movement. The laser was switched on at the moment the robot started moving. The laser was switched off once the robot had been moved by the processing distance in the z direction. The movement was repeated after moving horizontally (and vertically) to a new cladding spot.

The ceramic structures manufactured in this set of experiments are shown in **Figure 2**. Vertical structures were built in all cases, but it is clear that the columns were much smaller compared to the processing distance for robot velocity of 10 mm s^{-1} or higher. Only for a robot velocity of 5 mm s^{-1} do the YSZ columns have quite precise height Δ_z.

The columns are dark grey, except the white tip of the column. A grey shading of the YSZ can be attributed to oxygen vacancies caused by processing at a high temperature under an inert argon atmosphere and rapid quenching to well below 1000 °C. This observation therefore suggests either rapid heat dissipation within the column base or a very limited overheating of the melt pool. As rapid heat dissipation is unreasonable for the thermal barrier coating material (heat conductivity $\lambda_{YSZ} \approx 2$ W m^{-1} K^{-1}), we assume that just enough energy was supplied for column built-up. Taking the estimated minimal column diameter into account this would result in a rather poor energy efficiency of 11%.

Nevertheless, column diameters are generally larger than the expected 200 µm. A widening of the diameter is particularly

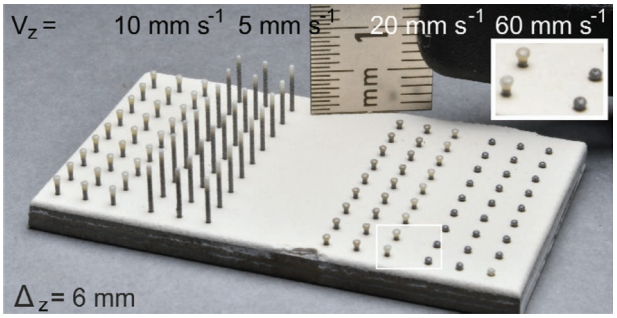

Figure 2. Laser cladded YSZ columns processed at different vertical robot velocities with 20 W laser power on APS YSZ on steel substrate.

observed for faster robot velocities and at the tips of the columns. The color of the tips is mostly white, which indicates the full oxidation of the YSZ. In contrast to the prior case, this can be attributed to significant overheating and a slow cool down. This might be due to the laser heating of the tips for a longer period of time during the movement of the cladding nozzle to the end position, while no significant further deposition of the powder takes place. No significant powder deposition is assumed because for higher robot velocities the column tip is far below the powder focal plane for a long period of time. In such situation, the molten material may be able to flow down and widen the tip (close-up image in Figure 2). In addition, the upward powder focus position allows impacting powder particles to arrive at the side of the column (by the confocal angle of the nozzle), possibly resulting in more powder particles sticking to the side and further widening the tip. In conclusion, for the laser parameters in this experiment robot velocities >5 mm s^{-1} lead to tiny columns with heights well below the processing distance and a huge surplus of energy until the end of the cladding process, while for a robot velocity of 5 mm s^{-1} the energy input in the process seems to be well balanced with the energy demand for column growth.

For the development of the TBCs, densely packed columns are required that form a coating with coating heights in the order of 1 mm and below. Columns were therefore arranged alongside each other in narrow patterns and the processing distance Δ_z was lowered with processing parameters slightly changed, maintaining a robot velocity of $v_z = 5$ mm s^{-1}. The distance between the columns (from column center to column center) in x–y plane of the substrate was initially set to $\Delta_{xy} = 0.5$ mm. The laser power was lowered to 15 W to reduce the risk of overheating, as indicated by the white colored column tip and the assumable smaller heat affected zone in the porous YSZ. These changes had no obvious effect on the column dimension.

In the cross section (**Figure 3**) columns manufactured at different Δ_z are shown. The cross sections show that the columns are dense, and each column has a constant diameter along column height. The columns are not connected to each other. The different diameters seen in Figure 3 might be attributed to the slightly off-center positions of the cross sections. By minimizing the column distance Δ_{xy} (in the substrate plane), the column diameter was estimated at slightly <450 µm, since for a Δ_{xy} of <450 µm the column pattern shows artefacts and thus the contact of the columns is assumed. For $\Delta_{xy} = 450$ µm

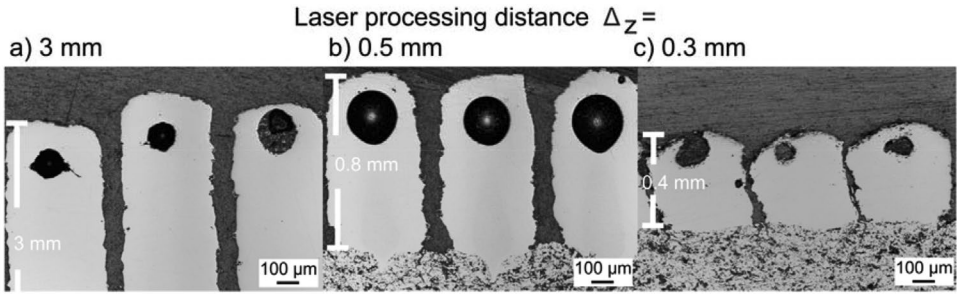

Figure 3. Laser-cladded YSZ columns processed at a robot velocity of 5 mm s^{-1} with a laser power of 15 W and a different vertical processing distance Δ_z on porous APS YSZ.

corresponding to the approximate column diameter, the energy demand for the buildup of the 5 mm column is up to 12.6 J (≈1.6 J for the formation of the initial melt pool and each 2.2 J mm^{-1} of column height). Compared to the total input of 24 J this indicates a quite acceptable loss of below 50% by beam scattering and the dissipation of heat.

The columns exhibit good adhesion to the APS YSZ coating, as a funnel of dense YSZ links the column to the porous coating (Figure 3 bottom). The powder efficiency was calculated at 8% by dividing the column mass by the powder mass fed during processing (assuming a column height of 6 mm, a constant diameter of 450 µm, a feed rate of 3.6 g min^{-1}, and constant robot velocity of 5 mm s^{-1}). A spherical pore is visible in the tip of the column. This pore might be formed by trapping porosity from the porous feedstock during the rapid cooldown of the tip after the laser is turned off under an argon flow.

By varying Δ_z the aim was to adjust the column height in accordance with the changes in Δ_z, as seen in previous experiments. Three observations are particularly worth noting. First, while for 3 (Figure 3) and 6 mm (previous experiment, 5 mm s^{-1}) the column height and the processing distance are more or less the same, for a lower Δ_z (0.5 mm, 0.3 mm) the column height is essentially higher than the Δ_z. Second, during column manufacturing where Δ_z = 0.3mm and Δ_z = 0.5 mm, the focal plane remains slightly below the substrate surface, although column growth is possible. This might be caused by the substantial powder supply above (and below) the focal plane. Third (from a previous experiment), the column height reached 6 mm in height, while the focal plane was not higher than 5 mm above the surface, which was also in accordance with the powder supply above the focal plane. Additionally, it is assumed that for low processing distances the robot was unable to reach the programmed vertical velocity of v_z = 5 mm s^{-1}, which is suitable for continuous column processing, due to the short accelerating and decelerating distances. In fact, for short distances the travel time of the robot, and thus the time at which the laser is turned on is much longer than expected while dividing the programmed velocity by the processing distance. In other words, a significant amount of energy is available for column build up exceeding the robot movement of Δ_z.

To determine the extent to which column growth is possible above and below the focal plane, experiments with a stepwise robot movement and with a pulsed energy supply were performed for discrete focal plane positions. For stepwise processing, the robot was moved to the starting position (with a specific focal plane position relative to the substrate surface). For a fixed position, the manufacturing of the column starts with a single laser pulse of 0.2 s. After one pulse, the robot moves by Δ_{xy} to further manufacturing positions. After some time (1–2 s), the robot horizontally returns to the initial manufacturing position and is raised vertically by one step (step size: 0.5 or 1 mm) to apply a second laser pulse. The focal plane of the robot rises step by step. By repeating the movements, with vertical steps and laser pulses, "column growth" is finished after seven laser pulses (and six vertical steps).

Images in **Figure 4**a show that stepwise processing by laser pulses results in the manufacturing of a homogeneous column 1 mm below and 1 mm above the focal plane at a fixed robot position. The column images are aligned with the arrows indicating the position and movement of the focal plane, relative to the column shown. For columns one and four, which can be seen in Figure 4a, single processing steps are outlined in detail in Figure 4b,c. The columns were divided into grown parts per laser pulse. Starting the column processing with a focal plane of 0.5 mm above the sample surface, a homogeneous column growth is visible in the bottom part of the column (First column, Figure 4a. By repeated movement and laser pulses the column grows further, but the growth rate is higher than the robot step. Therefore, after a few pulses the column grows significantly above the focal plane resulting in inhomogeneous droplet synthesis, for example, for the laser pulses 4–7.

Upon detailed analysis, the first grown part of column one is homogeneous and was estimated at ≈0.8 mm growth in height during a laser pulse of 0.2 s. For this column, the focal plane was above the substrate for the first laser pulse. The laser was therefore able to preheat and partly melt the powder particles in the powder focus and result in a melting pool (with the remaining transmitted laser energy). For the first laser pulse in particular, there was significant column growth as the focal plane (and thus the powder focus) was above the substrate and molten powder particles commonly exit radially at the confocal power focus (as shown by Wen at al.[14]). As the step size was shorter than the grown part per laser pulse, the focal plane of the robot was below the "grown" column surface after several laser pulses. This resulted in droplet formation (visible in the upper part of the first column). For the latter laser pulses, the column was above the focal plane, meaning the surface of the column could reach high temperatures as there were less powder particles shielding the laser radiation. A small number of particles might reach the tip by

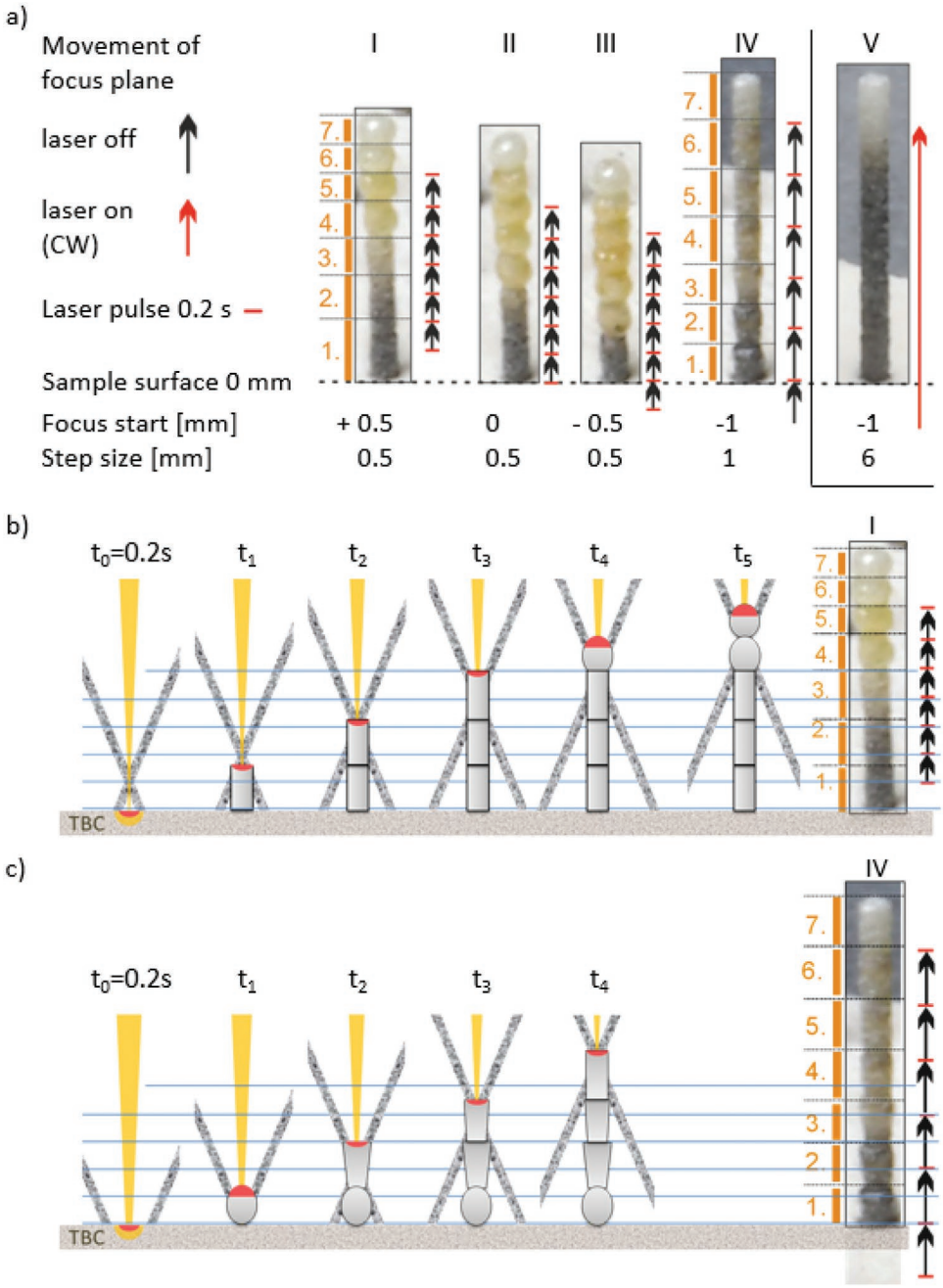

Figure 4. Laser-cladded YSZ columns manufactured by 0.2 s infrared laser pulses (15 W) and a repeated stepwise vertical focal plane movement (robot movement), which is illustrated by black arrows (laser off during movement); the red arrow corresponds to column processing at a continuous velocity and laser irradiation (laser on during movement), a variation of the focal plane at the start position (focal plane = +0.5 mm above to –1 mm below sample surface) and a step-size variation (0.5 and 1 mm) column comparison a) and detailed schematic view of single processing steps for b) 0.5 mm and c) 1 mm robot steps.

gas flow turbulences or redirection by collisions. These particles reached the edge of the melting pool sideways. The gas released from porous particles might introduce a heat barrier, which caused overheating of the newly deposited material. The surface tension of the newly deposited material led to the formation of droplets. This effect might be partially comparable to water droplets on a heating plate. By lowering the starting position of the focal plane the column tip grew earlier above the focus resulting in more droplets (second and third column in Figure 4a).

The step size was increased to 1 mm with the focal plane starting at 1 mm below the surface (fourth column in Figure 4a and outlined in Figure 4c). Column growth started with the first pulse of the laser through the formation of droplets, as the column growth (for the first pulse even the substrate surface) was above the focal plane. During stepwise column synthesis

with a 1 mm step size (1 mm per laser pulse), the column growth of ≈0.8 mm per laser pulse (0.2 s) was lower than the vertical stepwise movement of the robot, meaning the growing column tip moved from below to in focal plane position step by step. As a result of the latter laser pulses (for laser pulses 5–7), the column growth was homogeneous. These experiments showed that column synthesis with continuous laser and robot movement (fifth column in Figure 4) was preferable. Stepwise processing needed further parameter variation to achieve a constant column growth and diameter. Homogeneous column manufacturing could be assumed within a 1 mm processing window around the focal plane.

2.2. Thermal Cycling Performance of Columnar YSZ Laser TBCs

For thermal cyclic testing in a burner rig facility, thermal cycling samples were coated with a common Ni-based bond coat and a thin APS porous YSZ top coat. The second top coat layer was laser-cladded columnar YSZ coating (Clad2Z coating). To apply the coating, columns were arranged in an ideal packing with a minimum distance of 450 µm between the columns. Samples with two laser coating thicknesses were manufactured by setting the processing heights at $\Delta_z = 0.4$ mm and $\Delta_z = 0.15$ mm.

In **Figure 5**a,b, a homogeneous Clad2Z coating is visible. Taken from the cross sections (Figure 5d,f,h), this results in a Clad2Z coating thickness of 450 or 300 µm respectively. Column heights measured in cross sections after thermal cycling show low standard deviation (Table 2). As all columns are processed one after another, this shows the high repeatability of the process. It is particularly worth noting that the Clad2Z coating process also allows the curved edge of the sample, to be coated (Figure 5b).

Samples were cycled to failure in a burner rig facility to evaluate the thermal cycling performance. After thermal cycling, a failure comparable to conventional APS top coat TBCs or double-layered SPS TBCs with a similar thickness of ≈500 µm was observed. Top coat delamination was found at the APS YSZ bond coat interface or within the APS interlayer close to the interface. This was visible in the cross sections and from the blue color of the oxide layer in top view (Figure 5). This failure mode at the bond coat interface was more dominant in case of the samples thermally cycled at 1300 °C maximum top coat temperature (Figure 5c,d). This observation could be attributed to the smaller temperature gradient as temperature gradients induced additional peak stresses at the beginning of transients in thermal cycling that tended to shift formation of critical cracks into the TBC layer.[15,16]

It is obvious that the columns still have adhesion to the APS YSZ coating and show no cracks at all. Cracking in the YSZ top coat is only visible within the porous APS coating. For thinner laser top coats of 300 µm (Figure 5g,h), buckling in the center of the sample is visible. This buckling is in line with the failure of columnar suspension plasma sprayed TBCs.[6,17]

As previously suggested, the color of the top coat changes from black to yellow, due to a reduced concentration of oxygen vacancies. We assume that the material is fully oxidized during the first heat treatment in the burner rig facility, thus changing to the bright color. Aside from visible changes of the top coat,

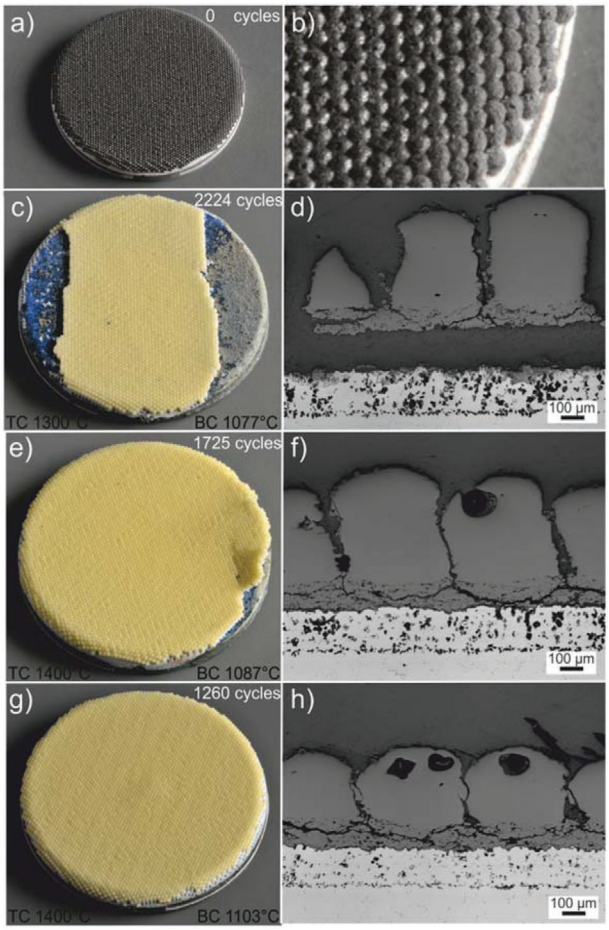

Figure 5. Top view and cross section of thermal cycling samples with double-layered Clad2Z and APS YSZ top coat in a,b) as-manufactured state, c,d) thermally cycled at 1300 °C top coat temperature (TC), e,f) thermally cycled at 1400 °C with 450 µm Clad2Z top coat, and g,h) thermally cycled at 1400 °C with a 300 µm Clad2Z top coat; average bond coat temperatures (BC) and number of cycles to failure (cycles) added by annotations (layer thicknesses presented in Table 2).

XRD reveals tetragonal YSZ in as-manufactured, tetragonal, and cubic phase after thermal cycling, which is consistent with the literature.[18]

Results of TBC lifetime in burner rig tests, as calculated from the number of cycles and the dwell time at high temperature, are presented in **Figure 6** as a function of the reciprocal bond coat temperatures. In addition to the results from the present study (circular symbols) data is shown for some relevant reference systems: single layer porous APS coatings (black line), double layer coatings with columnar SPS top layer (square symbols), columnar single layer PS-PVD coatings (diamond symbols), and commercial state of the art columnar EB-PVD coatings (blue shading). All cited TBC sample tests are performed on the same burner rig facility with 5 min dwell time at high temperature and the surface temperatures of ≈1400 °C, except commercial EB-PVD coatings with ceramic layer thicknesses well below 300 µm.[19]

The Arrhenius type correlation is obvious in the logarithmic plot (Figure 6). The correlation is due to the thermally activated

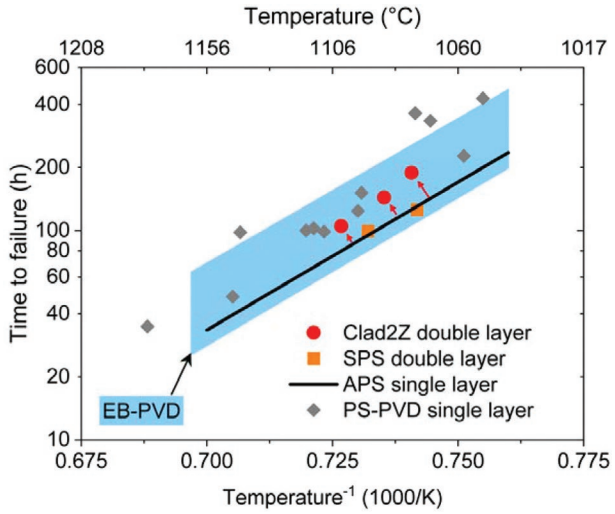

Figure 6. Results of burner rig tests for Clad2Z top coat TBCs (circular symbols) as a function of reciprocal bond coat temperature. Data for double layer top coat TBC samples with columnar SPS top coat layer (square symbols), single layer porous APS coatings (black line), typical range of results for commercial EB-PVD TBCs (blue shading), and columnar single layer PS-PVD coatings (diamond symbols).[19]

TGO growth and indicates TGO growth as the major driver of failure for the samples in the present and cited study. Along with the Arrhenius correlation of the TBC samples, the results from tests performed at different interface temperatures can be compared.

It is striking that the lifetime results of the Clad2Z double layer TBCs clearly outperform (improvement marked by red arrows in Figure 6) those of a standard single layered porous YSZ APS TBCs as well as those of double layer systems having APS YSZ interlayer combined with a columnar top layer applied by SPS. Clad2Z TBCs outperforming SPS TBCs is of special interest as these systems are similar in coating design and namely inspired the development of Clad2Z process as mentioned earlier. Results of columnar single layer coatings deposited by the PS-PVD process show in some cases significantly longer cyclic life. Nevertheless, this rather new technology up to now suffers from substantial complexity and cost.

Results of the Clad2Z TBCs are well within the performance range of commercial EB-PVD TBCs (data cannot be published in more detail for confidential reasons). This is remarkable as the typical lower thickness of the EB-PVD coatings implies a lowering of two important thermomechanical load parameters if the temperature gradient remains similar: not only the surface temperature is reduced but also the energy release rate on thermal cycling. Thereby, we may conclude that the columnar structure of the top coat effectively reduces the energy release rate during cycling while the toughness of the APS interlayer is not critically degraded by the laser processing. This conclusion is also supported by the Arrhenius type correlation of Clad2Z lifetimes, which is not changed upon delamination cracks shifting into the APS layer.

3. Conclusion

Additive manufacturing of ceramic YSZ columns on porous YSZ coatings by laser cladding with a confocal powder nozzle (Clad2Z) was found to perform well at a continuous vertical robot movement of v_z = 5 mm s^{-1}. Analysis of the obtained column cross section revealed dense YSZ columns with good adhesion to the porous YSZ layer underneath. Manufacturing parameter variations showed a flexible column height and stable column manufacturing within a processing window of 1 mm around the laser/powder focal plane. Stepwise column processing by single laser pulses and stepwise robot movement as well as possible pattern variation for structural design was also achieved.

Initial application of the YSZ columns manufactured by Clad2Z as an additional columnar top coat on a porous APS YSZ coating showed impressive results on thermal cycling performance. Thermal cycling samples with a conventional vacuum-plasma-sprayed bond coat, a thin conventional APS YSZ top coat, and a columnar Clad2Z top coat exceeded the performance of samples with a columnar suspension plasma spayed columnar top coat instead and also of conventional APS TBCs.

Established coating processes for the production of TBCs, such as EB-PVD and thermal spraying, are only suitable to a limited extent for coating small areas when a local failure on a high performance part needs to be repaired. With Clad2Z, processing on a small scale is possible, so that it is possible to repair TBCs[20] or metal components.[21] An additional advantage of using Clad2Z is that this avoids closing, for example cooling holes for turbine blades, due to single column manufacturing and precise control of the coated area. Aside from TBCs further applications can be assumed such as rapid ceramic prototyping,[1] repair techniques (even on a small scale), manufacturing contact layers for fuel cells, and further protective ceramic layers. Manufacturing hybrid ceramic and metallic structures, for example, top coat and bond coat might be a future topic worth investigating.

4. Experimental Section

Laser Setup: The laser cladding was performed using a multi-axis computerized numerical control (CNC) system, TruLaser Cell 3008 (Trumpf, Ditzingen, Germany), with a Nd:YAG laser (TruFiber 400, 12–400 W cw, Wavelength = 1064 nm). A coaxial jet nozzle, Coax 8 (ILT, Aachen, Germany), was used to deliver the powder by a fixed argon gas flow to the laser spot (Figure 1). The argon flow (20 l min^{-1})

Table 1. Thermal spray parameters.

System	Plasma Torch	Current [A]	Voltage [V]	Ar/H_2 [slpm]	Feeding Gas Ar [slpm]	Powder feeder	Pressure	Distance [mm]	Robot velocity [mm s^{-1}]
VPS	F4	640	70	50/9	1.7	15%	60 mbar	275	440
APS	Triplex Pro 210	420	90	46/0	2	20%	1 atm	200	500

Table 2. Thermal cycling sample parameters.

Letter In Figure 5	Top coat [µm]	APS Top coat [µm]	Bond Coat [µm]	Top coat temperature [°C]	Bond coat temperature [°C]	Cycles
c,d)	408 ± 11	108 ± 11	187 ± 10	1307	1077	2224
e,f)	447 ± 6	114 ± 13	181 ± 5	1408	1087	1725
g,h)	305 ± 26	117 ± 6	177 ± 11	1408	1103	1260
a,b)	≈450	≈110	≈160	–	–	0

and powder feed rate (3.6 g min^{-1}) of the powder feeder (GTV PF 2/2, Luckenbach, Germany) was set a few seconds before starting the cladding process in order to keep these parameters constant during processing. The commercial agglomerated and sintered yttria-stabilized zirconia powder Metco 233 B (Oerlicon Metco, Wholen, Switzerland) had a spherical microstructure with porous powder particles (nominal –45 + 22 µm).

Sample Preparation: The substrates for the laser cladding of the YSZ columns were YSZ-coated steel plates. Porous YSZ coatings on steel were manufactured by atmospheric plasma spraying using a MultiCoat facility (Oerlikon Metco, Wohlen, Switzerland) with a three-cathode TriplexPro 210 gun. All samples were grit blasted by F36 silica prior to plasma spraying. The thermal cycling samples were made of Inconel 738 (Doncaster Precision Castings – Bochum GmbH, Germany) with a diameter of 30 mm and a thickness of 3 mm. Thermal cycling samples were additionally coated with a bond coat prior to porous YSZ coating. The samples were coated with a 160 µm Ni-based bond coat followed by diffusion annealing and an APS YSZ coating (120 µm YSZ). The bond coat was applied by vacuum plasma spraying (F4 gun Oerlikon Metco, Wohlen, Switzerland) to achieve highly dense coatings with a low oxide content. Chemical compositions of alloys could be found in previous publications.[22,23] Thermal spray parameters are presented in **Table 1**.

Samples were analyzed by top view or metallographic cross section. The cross sections were ground in several steps and finally polished by 3 and 1 µm diamond suspension. They were analyzed by laser scanning microscope Keyence VK-9710 (Neu-Isenburg, Germany).

Thermal Cycling Setup: The samples were thermally cycled under a thermal gradient by a burner rig facility with gas flame heating of the front side and pressurized air cooling of the backside. Every 5 min, the heating process was automatically interrupted by 2 min of pressurized air cooling. The front-side temperature was set to 1300 or 1400 °C and measured by pyrometer (KT15, Heitronics, Wiesbaden, Germany) with a spot size of 12 mm, assuming an emissivity of $\varepsilon = 1$. The substrate temperature was set to 1050 °C and measured by a thermocouple in the thermal cycling sample. The bond coat temperature was calculated using the average front side and substrate temperature by assuming the linear thermal conductivity of the sample layers and by using the layer thicknesses measured in the cross section. The thicknesses were averaged using five laser images with ten measurement points per image. Errors intervals corresponded to the standard deviation of the mean values of each image. The thermal conductivities were assumed to be 1 W m^{-1} K^{-1} for YSZ layers, 37 W m^{-1} K^{-1} for the bond coat, and 26 W m^{-1} K^{-1} for the substrate. A detailed sample specification is provided in **Table 2**. For performance analysis, the samples were cycled until the sample showed at least 5 mm delamination or a significant deviation in the sample surface temperature occurred.[24] Metallographic preparation of the cycled samples was the same as for the laser cladding samples.

Acknowledgements

C.V. would like to give a special thanks to Martin Tandler for the introduction to and assistance with the laser cladding facility.

Open access funding enabled and organized by Projekt DEAL.

Conflict of Interest

The authors declare no conflict of interest.

Data Availability Statement

The data that support the findings of this study are available from the corresponding author upon reasonable request.

Keywords

additive manufacturing, energy generation, lasers, laser cladding, protective coatings

Received: January 17, 2022
Revised: March 10, 2022
Published online: April 25, 2022

[1] E. Toyserkani, A. Khajepour, S. F. Corbin, *Laser Cladding*, CRC Press, Florida, USA **2004**
[2] L. Zhu, P. Xue, Q. Lan, G. Meng, Y. Ren, Z. Yang, P. Xu, Z. Liu, *Opt. Laser Technol.* **2021**, *138*, 106915.
[3] F. Weng, C. Chen, H. Yu, *Mater. Des.* **2014**, *58*, 412.
[4] J. H. Ouyang, S. Nowotny, A. Richter, E. Beyer, *Ceram. Int.* **2001**, *27*, 15.
[5] Z. Li, M. Wei, K. Xiao, Z. Bai, W. Xue, C. Dong, D. Wei, X. Li, *Ceram. Int.* **2019**, *45*, 115.
[6] D. Zhou, D. E. Mack, P. Gerald, O. Guillon, R. Vaßen, *Ceram. Int.* **2019**, *45*, 1847.
[7] E. Bakan, R. Vaßen, *J. Therm. Spray Technol.* **2017**, *26*, 992.
[8] R. Siegel, C. M. Spuckler, *Mater. Sci. Eng., A* **1998**, *245*, 150.
[9] J. I. Eldridge, C. M. Spuckler, J. R. Markham, *J. Am. Ceram. Soc.* **2009**, *92*, 2276.
[10] J. I. Eldridge, C. M. Spuckler, *J. Am. Ceram. Soc.* **2008**, *91*, 1603.
[11] R. Vaßen, H. Kaßner, A. Stuke, D. E. Mack, M. O. Jarligo, D. Stöver, *Mater. Sci. Forum* **2010**, *631*, 73.
[12] Y. Zhang, D. E. Mack, G. Mauer, R. Vaßen, *Coatings* **2018**, *8*, 176.
[13] W. Ya, J. F. Hernández-Sánchez, B. Pathiraj, **2013**.
[14] S. Y. Wen, Y. C. Shin, J. Y. Murthy, P. E. Sojka, *Int. J. Heat Mass Transfer* **2009**, *52*, 5867.
[15] O. Trunova, RWTH Aachen, Diss., RWTH Aachen, Germany **2006**.
[16] S. Sundaram, D. Lipkin, C. Johnson, J. Hutchinson, *J.l of Appl. Mech.* **2013**, *80*, 1002.
[17] D. Zhou, O. Guillon, R. Vaßen, *Coatings* **2017**, *7*, 120.
[18] D. M. Lipkin, J. A. Krogstad, Y. Gao, C. A. Johnson, W. A. Nelson, C. G. Levi, *J. Am. Ceram. Soc.* **2013**, *96*, 290.
[19] R. Vaßen, E. Bakan, D. E. Mack, O. Guillon, *J. Therm. Spray Technol.* **2022**
[20] Y. Zhang, *Ruhr-Universität Bochum, Diss., 2015*, Ruhr-Universität Bochum, Bochum, Germany **2016**.

[21] S. Nowotny, S. Scharek, E. Beyer, K.-H. Richter, *J. Therm. Spray Technol.* **2007**, *16*, 344.
[22] C. Vorkötter, S. P. Hagen, G. Pintsuk, D. E. Mack, S. Virtanen, O. Guillon, R. Vaßen, **2019**, *92*, 167.
[23] C. Vorkötter, D. E. Mack, O. Guillon, R. Vaßen, *Surf. Coat. Technol.* **2019**, *361*, 150.
[24] F. Traeger, R. Vaßen, K. H. Rauwald, D. Stöver, *Adv. Eng. Mater.* **2003**, *5*, 429.